JOURNAL OF MATERIALS SCIENCE **34** (1999) 4065 – 4073

Phase transformations in a super ferritic stainless steel containing 28% Cr after nitrogen ion implantation

A. M. KLIAUGA, M. POHL
Institut für Werkstoffe, Ruhr-Universität Bochum, Universitätsstr. 150, IA 1-150, D-44780 Bochum, Germany
E-mail: pohl@wp.ruhr-uni-bochum.de

C. CORDIER-ROBERT, J. FOCT
Laboratoire de Métallurgie Physique, URA 234 USTL, 59655 Villeneuve d'Ascq Cédex, France

A super ferritic stainless steel with 28.12% Cr; 3.91% Ni; 2.44% Mo; 0.22% Mn; 0.35% Si; 0.01% C; 0.01% N was implanted with nitrogen ions at 60 and 100 keV with different implantation doses. The nitrogen distribution and the microstructure of the implanted layers were analysed by means of nuclear reaction analysis (NRA), Mössbauer spectroscopy (CEMS) and transmission electron microscopy (TEM). A nitrogen saturated austenite was formed at a lower implantation dose, this austenite led to the precipitation of α''-$Fe_{16}N_2$ nitrides and chromium nitrides by increasing the implantation dose and the implantation energy.

1. Introduction

Nitrogen ion implantation in stainless steels changes their surface properties purposefully, comprising their tribological, mechanical and corrosion behavior, due to the change of the chemical composition and the microstructure as for example the increase of dislocations and vacancy densities, the introduction of interstitial atoms and the precipitation of nitrides. The range of distribution of the implanted atoms and the distribution of radiation induced defects is influenced by the implantation parameters, as temperature, energy, implantation dose and the current density. The mobility of the atoms in the implanted target is the limiting factor to the final microstructure at the modified surface.

The ion implantation of austenitic stainless steels has been studied extensively [1–5], and the efforts focus on the formation of a nitrogen super saturated austenite, called γ_N or S-Phase, which improves the wear [6] and the corrosion resistance [7] of the nitrided surface. This metastable phase can be obtained below 400 °C, provided that the mobility of the chromium atoms is low enough to avoid the formation of CrN and γ'-Fe_4N nitride [8]. Nitriding at low temperatures has been a successful way to obtain a harder nitrogen rich layer without the formation of chromium nitrides, which are known to induce pitting corrosion.

There is a lack of information about the nitriding of ferritic stainless steels at low temperatures. In this paper, we investigate the microstructure of a nitrogen, ion implanted 28% chromium ferritic stainless steel using nuclear reaction analysis (NRA) to quantify the distribution of the implanted nitrogen and ^{57}Co Mössbauer spectroscopy (CEMS) and transmission electron microscopy (TEM) to identify the type of nitrides formed during the implantation.

2. Experiment

The ferritic stainless steel used had 28.12% Cr; 3.91% Ni; 2.44% Mo; 0.22% Mn; 0.35% Si; 0.01% C; 0.01% N (wt %). The specimen was a square plate having an edge length of 120 mm and a thickness of 5 mm. The average polycrystalline grain size was 130 μm. Before implanting the samples their surface was ground with emery paper to 1000 grid and electrolytically polished.

The ion implantation was performed under 60 keV with an implantation dose of 3×10^{16} and 1×10^{17} N^+/cm^2 at a beam current of 1.5 $\mu A/cm^2$ (samples IF-6-0.3 and IF-6-1) and under 100 keV with an implantation dose of 4×10^{17} and 1×10^{18} N^+/cm^2 at a beam current of 3.5 $\mu A/cm^2$ (samples IF-10-4 and IF-10-10). The temperature was kept close to 100 °C. Table I gives an overview of the samples.

The nitrogen profiles were performed by means of nuclear reaction analysis using the reaction $^{14}N(p, \gamma)^{15}O$ and a characteristic energy of 278.1 ± 1.06 keV.

The internal conversion electrons in the CEMS technique were detected by means of a 96% He-4% CH_4 gas flow proportional counter. The Mössbauer source was ^{57}Co in a rhodium matrix. Spectra recorded at room temperature were fitted according to a least squares procedure with a Lorenzian shape of Mössbauer lines. The velocity was calibrated by reference to an iron absorber.

Samples for TEM analysis were prepared by grinding and jet polishing on the target side with an electrolyte

TABLE I Implantation parameters of the sample: current density (μA/cm^2), energy (keV) and implantation dose (N$^+$/cm^2)

Sample	Current density (μA/cm^2)	Energy (keV)	Implantation dose (N$^+$/cm^2)
IF-6-0.3	1.5	60	3×10^{16}
IF-6-1	1.5	60	1×10^{17}
IF-10-4	3.5	100	4×10^{17}
IF-10-10	3.5	100	1×10^{18}

containing 100 ml perchloric acid, 200 ml glycerol and 700 ml methanol at $-16\,^{\circ}$C and 30 V.

3. Results and discussion

3.1. Nuclear reaction analysis

In a bcc iron structure the diffusion is faster than in a fcc iron structure, and the nitrogen solubility is lower. On the other hand, the high chromium content of the alloy should increase the nitrogen solubility, or better the affinity of the alloy to nitrogen, so that a greater amount of nitrogen could be absorbed and chromium nitrides could form as long as the chromium mobility was ensured [9, 10]. It is also known that chromium lowers the diffusivity of nitrogen [11].

The nuclear reaction analysis results are shown in Fig. 1. The implanted profiles indicate that the diffusion of nitrogen into the interior of the targets—which would cause a wider nitrogen distribution—occurred only at high dose, high energy ion implantation (100 keV; 1×10^{18} N$^+$/cm^2) and in a small scale. These profiles were close to the ones predicted by TRIM simulation [12]. Table II shows the predicted and measured values for the projected range R_P, its deviation ΔR_P and the calculated maximal nitrogen concentration, considering the nominal implantation dose.

During the ion implantation the implanted atoms collide with the target atoms and induce the formation of vacancies and dislocations. The collision cascade is transmitted in the closely packed directions in the crystal structure—for the bcc crystal this is the <111> direction. The generated dislocations are similar to dislocation structures of slightly deformed metals [13]. The extent of the defects in the case of nitrogen implanted in iron-chromium where the atomic mass relation is 1 : 4 can be considered as well distributed along the depth. Didenko *et al*. [14] measured the discordance density in α-iron after the ion implantation with C, Fe, W and Hf and Ar. They observed a shallow dislocation distribution after the implantation of C atoms whereas heavier atoms as W introduced a higher dislocation density with a major concentration close to the surface. The energy dissipated in those collisions led to a thermal spike that provides a local rearrangement of the defected structure. A redistribution of the implanted atoms to the region of major concentration of defects may occur [15] as well as the precipitation of nitrides. These processes are similar to the ones taking place during the deformation and recovering of metals.

Recovering in bcc structures, in which the substitutional and interstitial atoms are more mobile, occurs easily and faster so that a more extensive distribution of the nitrogen atoms and/or the precipitation of nitrides could be expected. An increase in implantation energy and implantation dose increases the number of subcascades, whose size (and the number of free defects and interstitial atoms produced in each of them) remains almost unchanged [16]. Thus the influence of the defect concentration on the nitrogen distribution should be higher at 100 keV and at higher implantation dose. In the case of the studied alloy, with approximately 29 at % Cr, the strong Cr-N interaction should influence the nitrogen distribution so that a nitrogen diffusion into the target was not accentuated.

TABLE II Implantation range values of the TRIM calculations and the obtained implantation ranges by means of NRA

		R_P (nm)	ΔR_P (nm)	N_{max} (at %)
TRIM-calculations	60 keV	64.6	35.9	—
	100 keV	106.3	50.4	—
Samples	IF-6-0.3	45	35	4
	IF-6-1	60	36	12.6
	IF-10-4	95	60	27
	IF10-10	110	90	42

3.2. Mössbauer spectroscopy

Fig. 2 compares the evolution of the Mössbauer spectra before and after the nitrogen ion implantation; the hyperfine parameters of the unimplanted and implanted ferritic stainless steel at room temperature are given in Table III. The untreated steel has a ferromagnetic environment with a magnetic splitting between 22.3 and 26 T. Earlier studies by Vincze and Campbell [17] described a reduction of the magnetic hyperfine field (H) in 2.6 T per chromium atom as first or second neighbour of an iron atom. Considering a random distribution of

TABLE III Mössbauer parameters of the unimplanted and implanted samples

Sample	Environment	*IS* (mm/s)	*H* (T)	*QS* (mm/s)	% *A*	Phase
Unimplanted	1	−0.02	26	0	40	$\alpha_{[Cr]}$
	2	−0.05	22	0	36	$\alpha_{[Cr]}$
	3	−0.02	19	0.04	18	$\alpha_{[Cr]}$
IF-6-0.3	E_0	−0.07	—	0	26	γ
	E_I	−0.04	—	0.39	18	$\gamma_{[N]}$
	1	−0.03	25.8	0	14	$\alpha_{[Cr]}$
	2	−0.09	22.5	0	42	$\alpha_{[Cr]}$
IF-10-4	E_0	−0.02	—	0	8	γ
	E_0'	−0.005	—	0.16	29	γ
	E_I	+0.07	—	0.42	44	γ_N
	E_{II}	+0.1	—	0.67	19	γ_N
	1	−0.05	28	0	21	$\alpha_{[Cr]}$
	2	−0.01	23	0	32	$\alpha_{[Cr]}$
IF-10-10	1	0.005	33.98	0	34	α
	2	−0.006	31.6	0	18	α'/α''
	3	−0.017	29.7	0	20	ε-$Fe_{2-3}N$
	4	−0.004	23	0	11	ε-$Fe_{2-3}N$
	5	+0.28		0.8	17	(Fe,Cr)N

Isomer shift *IS* (mm/s); magnetic hyperfine field *H* (T); quadrupole splitting *QS* (mm/s). Present phases in the analysed samples: chromium alloyed ferrite ($\alpha_{[Cr]}$); iron ferrite (α); nitrogen martensite (α'); α''-$Fe_{16}N_2$ nitride; austenite γ; austenite with nitrogen in solid solution ($\gamma_{[N]}$), nitrogen super saturated austenite (γ_N), ε-$Fe_{2-3}N$ nitride; (Fe, Cr)N nitride.

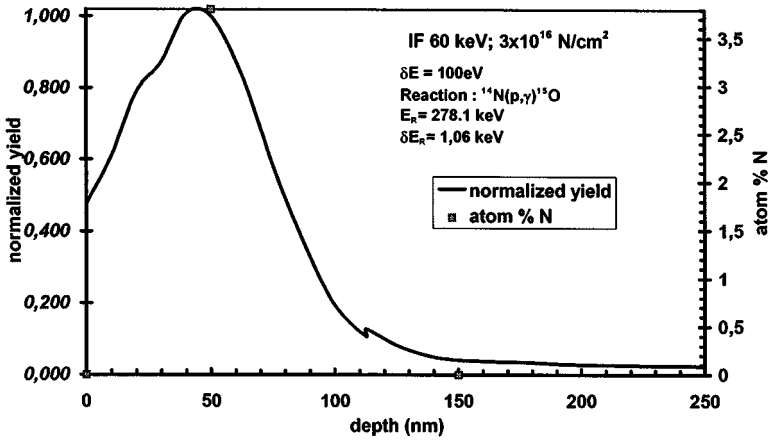

(a)

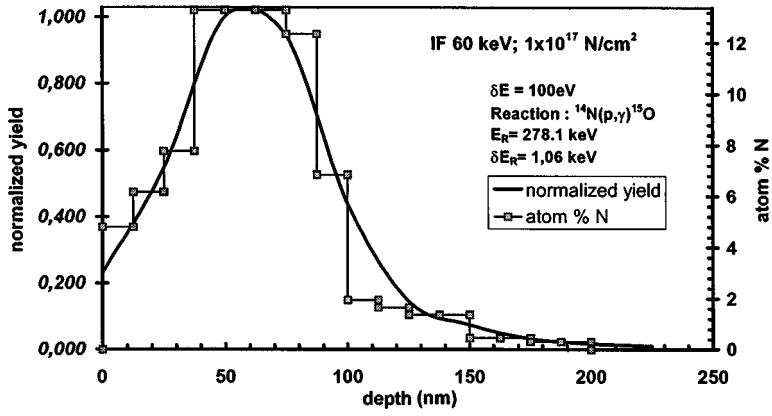

(b)

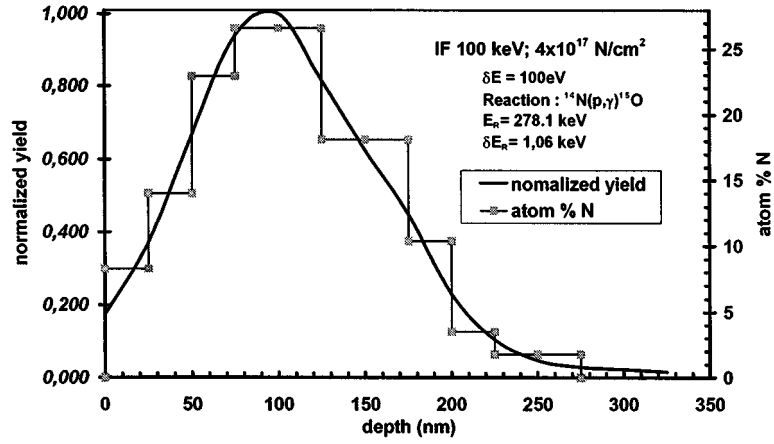

(c)

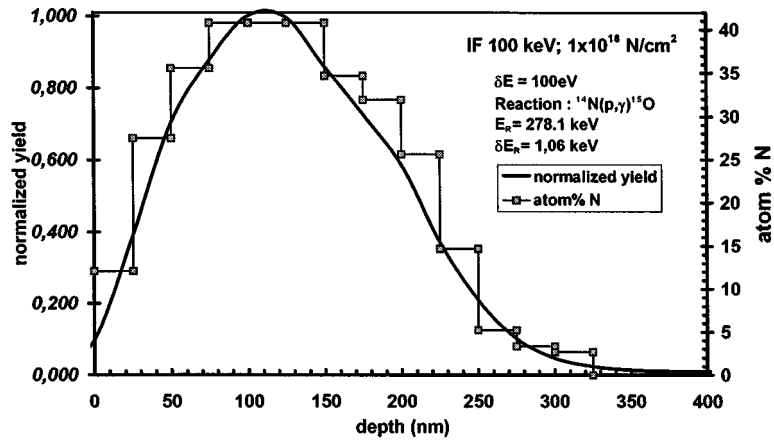

(d)

Figure 1 Nitrogen profiles of the implanted samples (—) measured (normalized yield) and (□) calculated values (at %): (a) 60 keV/3 × 10^{16} N^+/cm^2; (b) 60 keV/1 × 10^{17} N^+/cm^2, (c) 100 keV/ 4 × 10^{17} N^+/cm^2, (d) 100 keV/1 × 10^{18} N^+/cm^2.

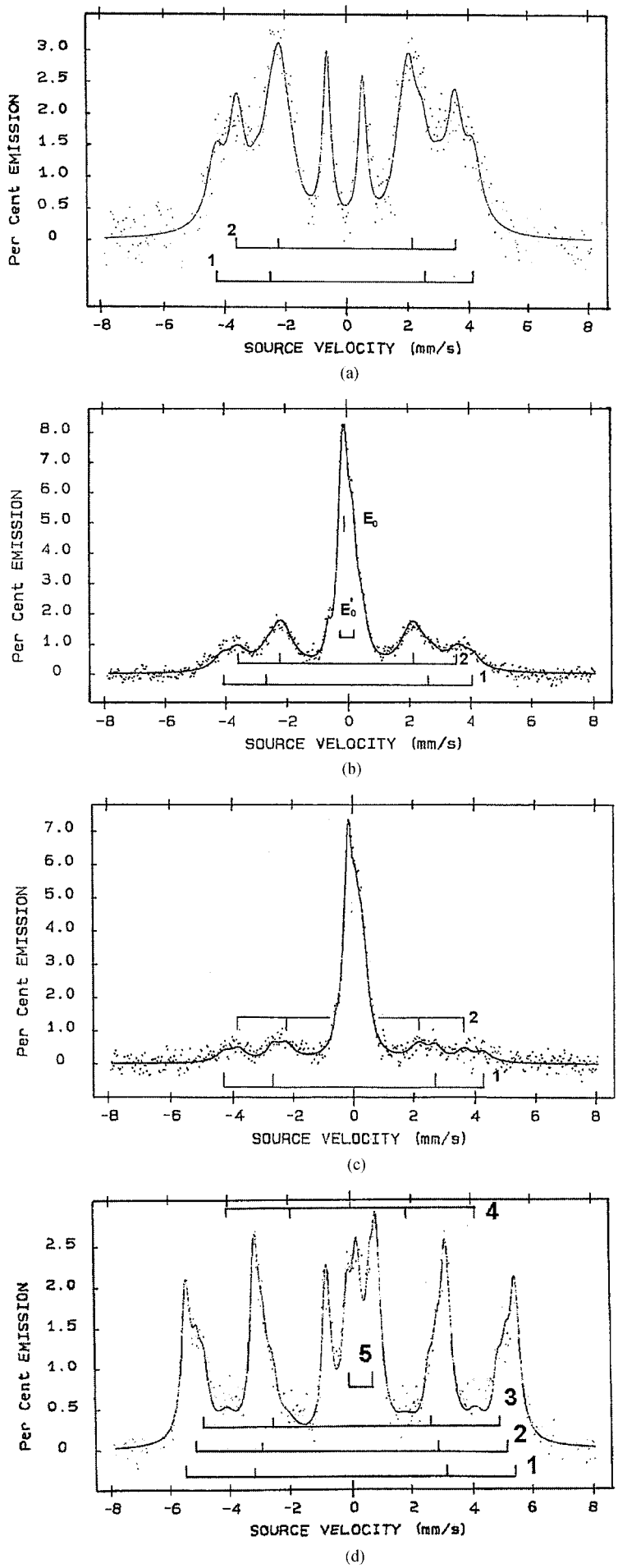

Figure 2 Mössbauer spectra of the unimplanted (a) and implanted samples: 60 keV, 3×10^{16} N^+/cm^2 (b); 100 keV, 4×10^{17} N^+/cm^2 (c) and 100 keV, 1×10^{18} N^+/cm^2 (d).

c at % Cr in the alloy ($c = 29$) the probability to have n chromium atoms in the first or second neighbourhood can be described as follows:

$$P(c, n) = \begin{bmatrix} 14 \\ n \end{bmatrix} \cdot c^n \cdot (1 - c)^{14-n} \qquad (1)$$

Comparing the random distribution and the fitting of the Mössbauer spectrum of the untreated sample (Fig. 3) it is possible to assume a nearly random distribution of chromium atoms in the alloy.

After the nitrogen implantation a paramagnetic environment appeared with typical values of nitrogen saturated austenite [2, 18] and quadrupole splitting values increasing from 0.39 mm/s at 60 keV and 3×10^{16} N^+/cm^2 to 0.67 mm/s at 100 keV and 4×10^{17} N^+/cm^2.

The formation of austenite after a nitrogen implantation in bcc iron with low chromium contents is not expected. Kopcewicz *et al*. [19] and Vredenberg *et al*. [20] determined the following nitride formation sequence during an ion implantation at temperatures around 150 °C: $\alpha \rightarrow \alpha'$ – martensite $\rightarrow a'' - Fe_{16}N_2 \rightarrow \varepsilon - Fe_{2-3}N$. Doping with chromium atoms may delay the formation of nitrides [21]. Nitriding of high chromium ferrite at temperatures around 500 °C usually leads to the precipitation of chromium nitrides followed by the precipitation of iron nitrides [22]. This last transformation can be followed up through a successive increase in the magnetic hyperfine field, showing that less chromium is allocated in the bcc iron structure and finally the formation of iron nitride environments can be detected. On the other hand a nitrogen addition at high temperatures (above 1000 °C) stabilises the austenite [23].

The paramagnetic region of sample IF-10-4 was measured once more to obtain detailed information about the nitrogen distribution in the austenitic region, as shown in Fig. 4. This detailed spectrum and the Mössbauer spectrum of sample IF-6-0.3 were fitted with two different iron environments, E_0 and E_0'. Both represent iron atoms without nitrogen neighbours. However, the substitutional neighbours more or less destroy the cubic symmetry of the fcc structure, giving rise to a quadrupole effect. Two other environments E_I and E_{II} could be determined as nitrogen neighbourhoods corresponding to iron atoms with one and two nitrogen nearest neighbours, respectively. The amount of nitrogen in the austenite X (in N atoms/100 Fe atoms) is given by the relation between the Mössbauer abundance

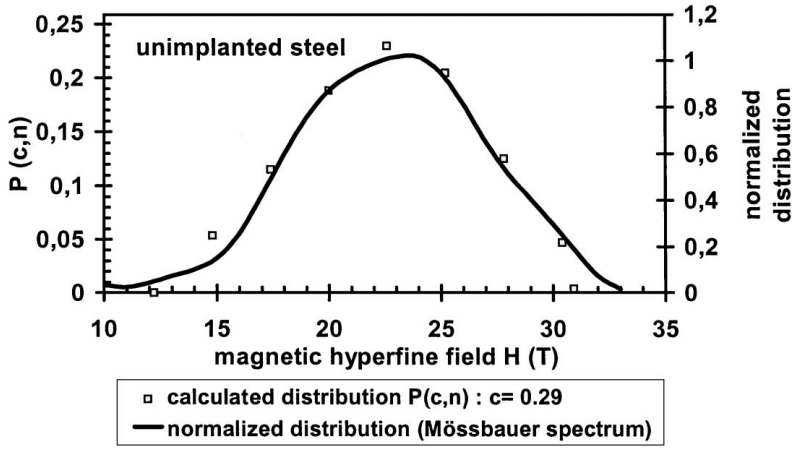

Figure 3 Probabilistic distribution of the Mössbauer environments of the unimplanted sample: (□) assuming a random distribution of chromium atoms according to Equation 1, $P(c, n)$ with $c = 29$, and (—) a fitted distribution of the magnetic hyperfine field environment.

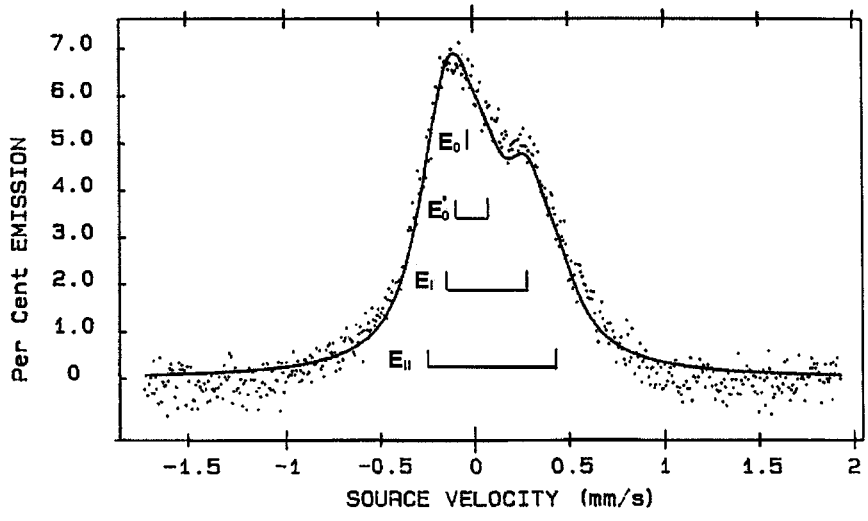

Figure 4 Detailed Mössbauer spectrum between −2 and 2 mm/s of sample IF-10-4.

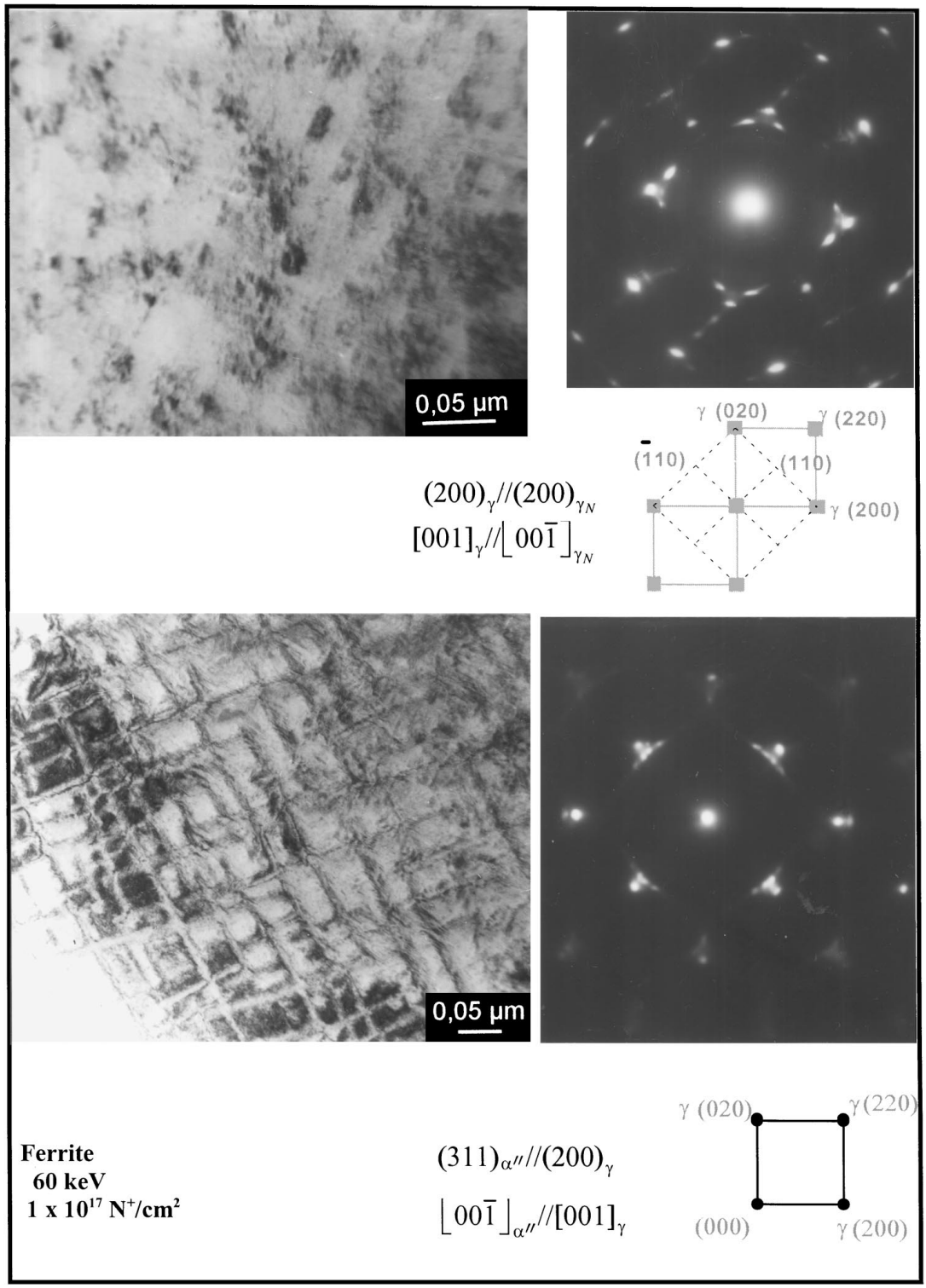

Figure 5 Ion implanted ferritic stainless steel at 60 keV and 1×10^{17} N^+/cm^2 (IF-6-1): fine austenite grains and α''-$Fe_{16}N_2$ nitride in austenite.

A_i of the E_i sites (corresponding to the one iron atom with i nitrogen nearest neighbours) [24]:

$$X = \left(\frac{A_{\mathrm{I}} + 2A_{\mathrm{II}}}{6} \right) \qquad (2)$$

After Equation 2 the expected nitrogen concentration in the austenite at 60 keV, 3×10^{16} N^+/cm^2 was 8 at % N and the maximal calculated nitrogen concentration by NRA was 4 at % N. The mass balance shows that 44% of the ferrite transformed into austenite, this is in agreement with the relative areas of austenite and ferrite in the Mössbauer spectrum. The magnetic hyperfine field of the ferrite did not change, and one can assume that all nitrogen was concentrated in the austenitic region. At 100 keV and 4×10^{17} N^+/cm^2 the nitrogen content in the austenite was 12 at % N according to Equation 2. However the NRA measurements showed that the maximal nitrogen content was 27 at % N. The excess of nitrogen should then interact with the chromium atoms. In fact, the magnetic hyperfine field of the ferrite environments increased at a higher implantation energy and dose, showing that chromium traps nitrogen, and that chromium nitride may have formed.

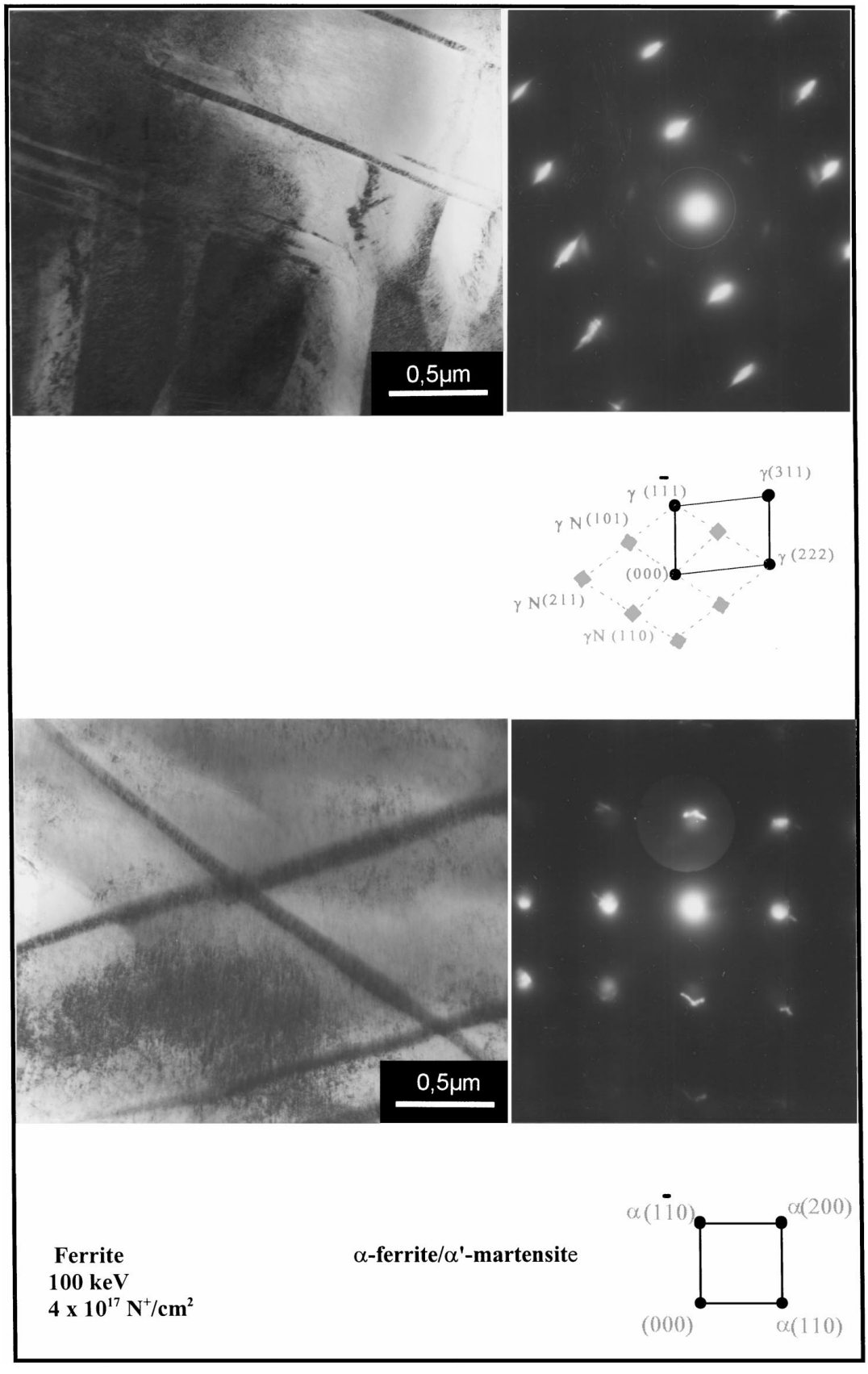

Figure 6 Ion implanted ferritic stainless steel at 100 keV and 4×10^{17} N^+/cm^2 (IF-10-4): austenitic/γ_N and ferritic/martensitic regions.

After the implantation at 100 keV and 1×10^{18} N^+/cm^2 a doublet characteristic for an MeN structure [25] (with $QS = 0.8$ mm/s and $IS = 0.28$ mm/s), where Me = (Fe, Cr) was measured, in other words CrN was formed. At this last implantation dose the austenite was not stable any more and the Mössbauer environments suggest the presence of ε-$Fe_{2-3}N$ nitride and the presence of a chromium free ferrite ($H = 33$ T). The sequence of transformations: $\alpha_{[Cr]} \rightarrow \gamma_N \rightarrow CrN + \varepsilon - Fe_{2-3}N + \alpha_{[Fe]}$ can be

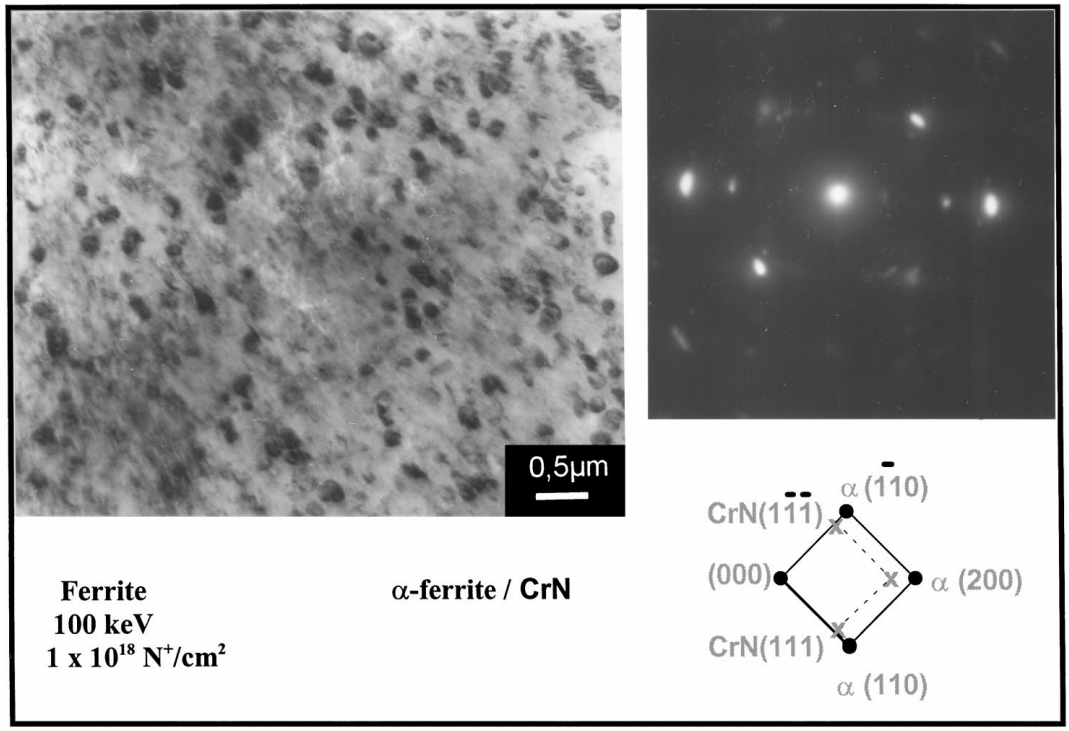

Figure 7 Ion implanted ferritic stainless steel at 100 keV and 1×10^{18} N^+/cm^2 (IF-10-10): CrN in ferrite.

understood under the assumption of a lower mobility of substitutional atoms at lower energy, and a lower implantation dose.

3.3. Transmission electron microscopy

Three samples were investigated by TEM: IF-6-1, IF-10-4 and IF-10-10. The sample implanted at 60 keV and 1×10^{17} N^+/cm^2 (IF-6-1) presented fine austenite grains and α''-$Fe_{16}N_2$ nitrides precipitated in austenite (Fig. 5) with the following crystallographic relationship with γ-Fe:

$$(310)_{\alpha''} // (200)_{\gamma}$$
$$[00\bar{1}]_{\alpha''} // [001]_{\gamma}$$

The α''-$Fe_{16}N_2$ nitride has a cell which is two times bigger than that of the ferrite, with a well known crystallographic relationship [26, 27] $(020)_{\alpha''} // (020)_{\alpha}$ and $[100]_{\alpha''} // [100]_{\alpha}$, which implies a coherency with α-iron. It is usually related with the ageing of nitrogen martensite, by the ordering of nitrogen atoms in bct iron [18, 28], but it can also precipitate in α'-iron independent of the martensite substructure, and act as a nucleation site to the γ'-Fe_4N nitride [29]. The formation of α''-$Fe_{16}N_2$ in austenite was not observed [30] so far although a martensitic transformation and the futher ordering of nitrogen atoms ($\gamma \rightarrow \alpha' \rightarrow \alpha''$-$Fe_{16}N_2$) exists.

After the implantation at 100 keV and 4×10 N^+/cm^2 (sample IF-10-4) nitrogen expanded austenite and ferrite with martensite needles (Fig. 5) were observed. At 1×10^8 N^+/cm^2 CrN precipitates in ferrite were detected (Fig. 6). These results are in agreement with the Mössbauer measurements.

Compared with the results of an ion implantation of pure iron reported in the literature [19, 20, 30], one should notice that the transformation $\alpha \rightarrow \alpha'$-martensite is crystallographically unlikely without a prior formation into fcc austenite. The γ-iron is unstable at room temperature and under the assumption that a thermal spike occurs during the implantation process, the rapid cooling could explain the formation of the observed martensite. In the high chromium alloy studied the austenite was stable. The first aspect to consider is the effect of alloying elements (N, C, Cr, Ni, Mn, Mo and Si) in lowering the martensite start temperature [31, 32]; this could explain the retention of austenite by a lower implantation dose. The second aspect to consider is the mobility of chromium atoms and therefore their reactivity to nitrogen. By increasing the implantation energy the chromium atoms reacted with nitrogen to form CrN, and the stabilising effect did not exist any longer, through the reduction of both nitrogen and chromium in the iron bcc solid solution.

4. Conclusions

The nitrogen ion implantation of ferritic stainless steel has yielded the following information about the influence of chromium in the nitride formation process: At 60 keV and 3×10^{16} N^+/cm^2 the formation of austenite prior to the martensitic transformation could be observed due to the reduction of the Ms temperature caused by the high chromium content and by the addition of nitrogen.

After rising the implantation dose and the energy, the density of radiation defects increased, their interaction with the substitutional atoms is enhanced and first chromium nitrides and then iron nitrides could form.

A crystallographic relation between austenite and α''-$Fe_{16}N_2$ was determined:

$$(310)_{\alpha''} // (200)_{\gamma}$$
$$[00\bar{1}]_{\alpha''} // [001]_{\gamma}$$

Acknowledgements

We would like to express our appreciation to M. A. T. GmbH, Dresden, for the ion implantation of the samples and to Dr. H. Schulte from the Physics Faculty of the Ruhr-Universität Bochum for the NRA analysis.

This work was partially supported by a Grand from the CNPq (Conselho Nacional de Desenvolvimento Científico e Tecnológico), Brazil.

References

1. C. CORDIER-ROBERT *et al*., *Mater. Lett.* **20** (1994) 113.
2. *Idem. J. Mater. Sci. Lett.* **13** (1994) 352.
3. D. L. WILLIAMSON *et al*., *Surface and Coatings Technology* **65** (1994) 15.
4. O. ÖZTÜRK and D. L. WILLIAMSON, *J. Appl. Phys.* **77** (1995) 3839.
5. X. LI *et al*., *Surface and Coatings Technology* **71** (1995) 175.
6. R. WEI *et al*., *J. Tribology* **116** (1994) 870.
7. P. A. DEARLEY *et al*., in Proc. Conf. Plasma Surface Engineering, PSE'88 (Garmisch-Partenkirchen, Germany, 1988)
8. K. ICHII, K. FUJIMURA and T. TAKASE, *Technology Reports of Kansai University* **27** (1986) 135.
9. H. K. FEICHTINGER, High Nitrogen Steels, HNS 1993 Proc. 3rd. Int. Conf. Kiev, Ukraine, 1993, p. 14.
10. K. FRISK, *Metall. Trans. A* **21A** (1990) 2477.
11. R. B. MC. LELLAN and R. FARRARO, *Acta Metall.* **5** (1977) 1217.
12. J. F. ZIEGLER and J. P. BIERSACK, in "The Stopping and Range of Ions in Solids" (Pergamon Press, NY, 1985).
13. R. S. NELSON, in Proc. of the NATO Advanced Study Institute on Radiation Damage Processes in Materials, Corsica, France, 1973, edited by C. H. S. Dupuy (Noordhoff International Publishing, Leyden, Netherlands, 1975) p. 261.
14. A. N. DIDENKO *et al*., *Surface and Coatings Technology* **65** (1994) 112.
15. P. D. TOWNSEND *et al*., in "Ion Implantation, Sputtering and Their Applications" (Academic Press, 1976).
16. N. MONCOFFRE and J. JAGIELSKI, *Surface and Coatings Technology* **65** (1994) 30.
17. I. VINCZE and A. CAMPBELL, *J. Phys. F: Metal Phys.* **3** (1973) 647.
18. J. M. R. GENIN and I. FALL, in Proc. 3rd. Int. Conf. High Nitrogen Steels—HNS '93, Kiev, Ulkraine, 1993, 261.
19. M. KOPCEWICZ *et al*., *J. Appl. Phys.* **71** (1992), 4217.
20. A. M. VREDENBERG *et al*., *J. Mater. Sci.* **7** (1992), 2689.
21. M. KOPCEWICZ *et al*., *J. Appl. Phys.* **78** (1995), 1312.
22. G. DLUBEK *et al*., in "Ausgewählte Untersuchungsverfahren in der Metallkunde" (Springer-Verlag, Wien, Austria, 1983) p. 247.
23. BERNS and S. SIEBERT, *Härterei Technische Mitteilung* **49** (1994) 123.
24. J. FOCT and R. ROCHEGUDE, *Hyp. Int.* **28** (1986) 1075.
25. J. J. GRABKE, C. UEBING and H. VIEFHAUS, in Proc. of High Nitrogen Steels—HNS 88, Lille, France, 1988, edited by J. Foct and A. Hendry (The Institute of Metals, 1989) p. 261.
26. R. D. GARWOOD and G. THOMAS, *Metall. Trans.* **4** (1973) 225.
27. Y. INOKUTI, N. NISHIDA and N. OHASHI, *ibid.* **6A** (1975) 773.
28. N. DE CRISTOFARO and R. KAPLOW, *ibid.* **8A** (1977) 35.
29. G. HINJOSA *et al*., *Scripta Materialia* **34** (1996) 141.
30. K. NAKAJIMA, S. OKAMOTO and T. OKADA, *J. Appl. Phys.* **65** (1989) 4357.
31. H. FLINKER and M. SCHIRRA, *Steel Research* **67** (1996) 328.
32. F. C. MONKMAN, F. B. CUFF and N. J. GRANT, *Metal Progress* **71** (1957) 94.

Received 18 April 1997
and accepted 16 February 1999